Ozone membrane contactor to intensify gas/liquid mass transfer and contaminants of emerging concern oxidation

Pedro H. Presumido [a,b,c], Rosa Montes [d], José B. Quintana [d], Rosario Rodil [d], Manuel Feliciano [c], Gianluca Li Puma [e], Ana I. Gomes [b,f], Vítor J.P. Vilar [a,b,*]

[a] *Laboratory of Separation and Reaction Engineering – Laboratory of Catalysis and Materials (LSRE-LCM), Chemical Engineering Department, Faculty of Engineering, University of Porto, Rua Dr. Roberto Frias, 4200-465 Porto, Portugal*
[b] *Associate Laboratory in Chemical Engineering (ALiCE), Faculty of Engineering, University of Porto, Rua Dr. Roberto Frias, 4200-465 Porto, Portugal*
[c] *Centro de Investigação de Montanha (CIMO), Instituto Politécnico de Bragança, Campus de Santa Apolónia, 5300-253 Bragança, Portugal*
[d] *Department of Analytical Chemistry, Nutrition and Food Sciences, Institute of Research on Chemical and Biological Analysis (IAQBUS), Universidade de Santiago de Compostela, Constantino Candeira S/N, 15782 Santiago de Compostela, Spain*
[e] *Environmental Nanocatalysis & Photoreaction Engineering, Department of Chemical Engineering, Loughborough University, Loughborough LE11 3TU, United Kingdom*
[f] *Laboratory for Process Engineering, Environment, Biotechnology and Energy (LEPABE), Faculty of Engineering, University of Porto, Rua Dr. Roberto Frias, 4200-465 Porto, Portugal*

ARTICLE INFO

ABSTRACT

A tubular porous borosilicate membrane contactor was investigated for ozone gas/water mass transfer and the removal of contaminants of emerging concern (CECs) in water. Ozone gas/water contact occurs on the membrane shell-side, which is coated with a photocatalyst (TiO$_2$-P25), as the ozone gas stream is fed from the lumen side and permeates through the pores generating micro-sized ozone bubbles uniformly delivered to the annular reaction zone where the contaminated water to be treated flows. Under continuous flow, water pH at 3.0 and temperature at 20 ºC, the volumetric mass transfer coefficient (K_La) ranged from 3.5 to 9.0 min^{-1} and improved with the increase of gas flow rate (Q_G, 1.5-fold from 0.15 to 1.0 Ndm^3 min^{-1}) and liquid flow rate (Q_L, 2.0-fold from 20 to 50 L h^{-1}), due to enhanced turbulence on the membrane shell-side and annular zone. The mass transfer efficiency was more pronounced as the Q_G decreased and the Q_L increased, which is advantageous for large-scale applications. The main resistances to ozone transfer were in the water phase boundary layer (53–76%) and in the membrane (24–47%; $k_M = (1.14 \pm 0.01) \times 10^{-4}$ m s^{-1}). For an ozone dose of 12 g m^{-3} and residence time of 3.9 s, removals ≥ 80% were achieved for 13 of 19 CECs spiked in demineralized water (each 10 μg L^{-1}), demonstrating the applicability of this membrane contactor for ozonation treatment. Photocatalytic ozonation (O$_3$/UVC/TiO$_2$) did not significantly improve the treatment performance due to the low residence time inside the contactor.

1. Introduction

Growing global health concerns due to the surge in urbanisation and industrialisation, leading to water contamination worldwide, are driving the ozone technology market globally. Ozonation is a technique most successfully applied in several fields of water/wastewater treatment [1], such as disinfection [2,3], oxidation of contaminants of emerging concern (CECs) [4–7], and removal of colour, odour, and taste [8]. Ozone (O$_3$) is usually produced by passing a stream of oxygen (O$_2$) through a corona discharge system, which provides energy to convert O$_2$

to O$_3$ [9]. A major obstacle to wider use of O$_3$ technology is the relatively high energy consumption (around 7.2–12.3 kW/kg O$_3$) [1], rather large footprint treatment unit, and operational issues related to the dispersion of ozone gas in water. Gas-liquid membrane contactors are an emerging alternative to traditional O$_3$ injection methods, such as fine bubble diffusers, for which O$_3$-liquid transport is a rate-limiting factor due to the size and distribution of O$_3$ bubbles. While the principles of direct gas-liquid mass transfer of O$_3$ into the aqueous phase are well understood, bubbling methods bear several disadvantages, such as locally inaccurate O$_3$ dosages due to short-circuiting, low ozone mass transfer rates from gas to liquid phase, foam formation in treatment reactors,

Nomenclature

$\frac{1}{k_G H}$	Mass transfer resistance in the gas boundary layer (s m^{-1}).
$\frac{1}{k_L}$	Mass transfer resistance in the liquid boundary layer (s m^{-1}).
$\frac{1}{k_M}$	Mass transfer resistance in the membrane matrix (s m^{-1}).
n_i	Number of bubbles of diameter d_{eq}.
$[CECs]_0$	CECs concentration in the feed liquid stream (μg dm^{-3}).
$[O_3^*]$	Ozone concentration in the liquid phase at saturation (g m^{-3}).
$[O_3]$	Dissolved ozone concentration at time t (g m^{-3}).
$[O_3]_G$	Ozone concentration in the inlet gas stream (g Nm^{-3}).
$[O_3]_{Gout}$	Ozone concentration in the outlet gas stream (g Nm^{-3}).
$[O_3]_L$	Dissolved ozone concentration in the outlet liquid stream at steady-state conditions (g m^{-3}).
a	Gas–water interfacial area of membrane per unit water volume (m^{-1}).
d_{32}	Sauter mean diameter (mm).
d_{eq}	Equivalent spherical bubble diameter (mm).
D_K	Knudsen diffusion coefficient (m^2 s^{-1}).
D_M	Effective diffusion coefficient of ozone in the membrane (m^2 s^{-1}).
D_{O3}	Diffusion coefficient of ozone in the gas phase (m^2 s^{-1}).
Dw_{O3}	Diffusion coefficient of ozone in water (m^2 s^{-1}).
d_{pore}	Mean pore diameter (m).
H	Henry coefficient.

Ha	Hatta number.
k_d	Self-decomposition constant of ozone (s^{-1} or min^{-1}).
k_G	Mass transfer coefficient in the gaseous phase (m s^{-1}).
k_L	Mass transfer coefficient in the water phase (m s^{-1}).
K_L	Overall mass transfer coefficient based on water phase (m s^{-1}).
$K_L a$	Volumetric mass transfer coefficient based on water phase (s^{-1} or min^{-1}).
k_M	Mass transfer coefficient in the membrane (m s^{-1}).
k_{O3}	Rate constant of the direct reaction between O$_3$ and the pollutant (M^{-1} s^{-1}).
M	Molar mass of ozone (g mol^{-1}).
MTE	Mass transfer efficiency (%).
OD_I	Inlet O$_3$ dose rate (g m^{-3}).
Q_G	Gas flow rate (Ndm^3 min^{-1}).
Q_L	Volumetric water flow rate (L h^{-1}).
R	Ideal gas constant (J K^{-1} mol^{-1}).
Re	Reynolds number.
T	Temperature (ºC or K).
TOD	Transferred ozone dose (g m^{-3}).
Δx	Membrane thickness (mm).
ε	Porosity of the membrane (%).
ε_G	Gas holdup (%).
τ	Hydraulic retention time (s).
τ_p	Pore tortuosity.

bubble coalescence and uneconomic off-gas recovery (mainly O$_2$) [1]. Moreover, conventional ozonation systems result in the need to use deeper tanks to obtain a higher dissolution efficiency of ozone gas into the water, as also as unconsumed/unreacted ozone losses and, consequently, higher operational costs and footprints.

Contrary to the basic principles of separation membranes, membrane contactors do not offer any selectivity, working just as a convenient barrier between the two phases, keeping them separated and allowing their contact in a large (as compared to volume) and well-defined interfacial area [10]. Compared with direct gas reactor, membrane reactor has the following advantages [11–15]: (i) the specific surface area of membrane contactors is much higher than in conventional contactors and may result in a higher volumetric mass transfer coefficient ($K_L a$); (ii) microscale bubble operation that prevent foaming phenomena; (iii) greater control on the dosing of ozone to the water; (iv) reduced losses of unreacted ozone; (v) scale-up to almost any size is easily possible by adding modules of the same type and size without losing transfer efficiency since a constant O$_3$ concentration can be established at the gas/liquid interface. Also, no changes in the specific energy dissipation are caused, which is crucial in the scale-up of direct gas reactors, and membrane reactors have a small footprint. The membranes can be used in small cross-section contactors with high linear flow rates, resulting in compact units with good plug-flow characteristics. In addition, membranes can be functionalised with nanoparticles or catalysts to improve membrane performance (nano-enhanced membranes) and the removal of water contaminants by catalytic ozonation [16–19]. This approach has proved successful in recent research, e.g., Mansas et al. [18] demonstrated the enhanced catalytic ozonation activity of a commercial nanofiltration ceramic membrane functionalized with mesoporous maghemite (γ-Fe$_2$O$_3$), also Liu et al. [17] applied a CuMn$_2$O$_4$/g-C$_3$N$_4$ catalytic ceramic membrane that increased more than 3-fold the degradation rate of benzophenone-4 when compared to O$_3$-only, and Lee et al. [16] developed a Ce-doped TiOx ceramic membrane that proved to be effective in degrading and mineralizing a mixture of micropollutants with low specific O$_3$ consumption.

In the present study, a novel ozone membrane contactor is proposed to intensify ozone gas/water mass transfer and, simultaneously, allow the use of light and catalyst to activate ozone in a single unit. In the tubular porous borosilicate membrane distributor, the O$_3$ stream is fed by the lumen side and quickly delivered to the liquid through "virtually" unlimited dosing points along the membrane length. An outer quartz tube allows light penetration through the annular reaction zone (ARZ), where the membrane shell-side is coated with titanium dioxide (TiO$_2$-P25). Such configuration allows the O$_3$ that is being dosed through the membrane pores to have a pseudo-uniform and direct contact with the active catalyst sites. This technological approach enables a more homogeneous distribution of the injected gas, generating O$_3$ microbubbles in the water and increasing the rate of ozone mass transfer, thus improving the reaction with the pollutants, reducing O$_3$ consumption and avoiding, at the same time, catalyst deactivation. Also, the helical water flow induced by the location of the inlet/outlet pipes (at opposite ends and tangentially to the quartz tube), has proven to improve the transport of fluid particles throughout the reactor and to promote intense macromixing dynamics [20]. This unique fluid dynamics, where contaminated water swirls around the membrane, enables longer contact time for the fluid particles to interact with O$_3$ bubbles and reduces local points near the membrane shell where higher O$_3$ concentrations occur, thus contributing to mass transfer. The increased performance of the proposed membrane contactor was assessed by measuring the volumetric mass transfer coefficient ($K_L a$), determined in continuous mode from a mass balance for O$_3$ in the gas and the liquid phases, considering the water pH and temperature (T), the O$_3$ concentration in the gas phase ([O$_3$]$_G$), the liquid (Q_L) and gas (Q_G) flow rates. Furthermore, the mass transfer efficiency (MTE), i.e., the fraction of O$_3$ that dissolves into the aqueous solution, was also determined. Lastly, also in continuous mode, the ozone membrane contactor was applied to treat a mixture of 19 CECs spiked in demineralized water at low concentrations (10 μg L^{-1}) to simulate the concentrations and the range of contaminants typically found in water and wastewater. The primary aim was to determine CECs degradation efficiency envisaging its application in

water/wastewater treatment.

2. Materials and methods

2.1. Chemical reagents

The O_3 probe was validated by the iodometric method with the use of potassium iodide (KI, Merck), sodium thiosulfate ($Na_2S_2O_3$, Pronalab), and amide (Sigma). In addition, the 2% KI solution was used to destroy any remaining O_3 in the outlet gas stream. Sulfuric acid (H_2SO_4, Pronalab) and sodium hydroxide (NaOH, Merck) solutions were used to adjust the solution pH. Titanium dioxide Aeroxide® P25 (TiO_2-P25, Evonik, Germany) $\geq$ 99.5% (w/w) purity was used as the photocatalyst, and the surfactant Triton™ X-100 (Sigma-Aldrich) was used in the preparation of the TiO_2-P25 suspension for membrane coating. Ultra-pure water (Millipore Direct-Q®, 18.2 MΩ cm^{-1} at 25 °C) was used to prepare all solutions and demineralized water-DW (Panice®) was used in all tests. The nineteen CECs applied in DW to investigate the performance of the ozonation system were supplied by Sigma-Aldrich, namely: 17α-Ethynylestradiol (EE2), 17β-Estradiol (E2), Acesulfame K (AC-K), Atenolol (ATNL), Bisoprolol (BSPL), Carbamazepine (CBZ), Carbamazepine 10,11-epoxide (CBZ-EPX), Diclofenac (DCF), Diethyltoluamide (DEET), Diuron (DRN), Heptafluorobutyric acid (PFBA), Irbesartan (ISTN), Losartan (LSTN), Melamine (MLN), Pentadecafluorooctanoic acid (PFOA), Nonafluoro-1-butanesulfonic acid (PFBS), Saccharin (SCH), Trifluoromethanesulfonic acid (TFMS) and Valsartan (VSTN).

Further details on the CECs can be found in Table S1, in the Supplementary Information file.

2.2. Lab-scale prototype

The schematic diagram of the lab-scale prototype is shown in Fig. 1. The apparatus consists of an ozone system and an ozone membrane reactor.

2.2.1. Ozone system

O_3 was generated from oxygen (O_2, 99.995% supplied by Air Liquide) by a BMT 802 N generator with a production capacity of up to 4 g O_3 h^{-1} (at 100 g Nm^{-3}, 20 °C). The input gas flow rate (Q_G = 0.15–1.00 Ndm^3 min^{-1}) was controlled with the aid of a digital mass flow meter (Alicat Scientific). The O_3 concentration in the gas flow ($[O_3]_G$ = 20–80 g Nm^{-3}) was controlled by changing the power input to the O_3 generator and was monitored with an O_3 analyser (BMT 964). Before passing through the analyser, the residual O_3 leaving the reactor passes through a column to separate the liquid and gas phase and is directed to a sample gas dehumidifier (BMT DH3b). After this, the gas phase was vented through the catalytic O_3 destruction unit (Heated Catalyst BMT) and sequentially to an O_3 destroyer bottle (containing a 2% KI solution) before going into exhaustion. The concentration of O_3 in water was monitored using a measuring cell AQC-D12 with a reference electrode for ozone (Grundfos Alldos) connected to a controller Conex DIA-1 (Grundfos Alldos). According to the manufacturer's
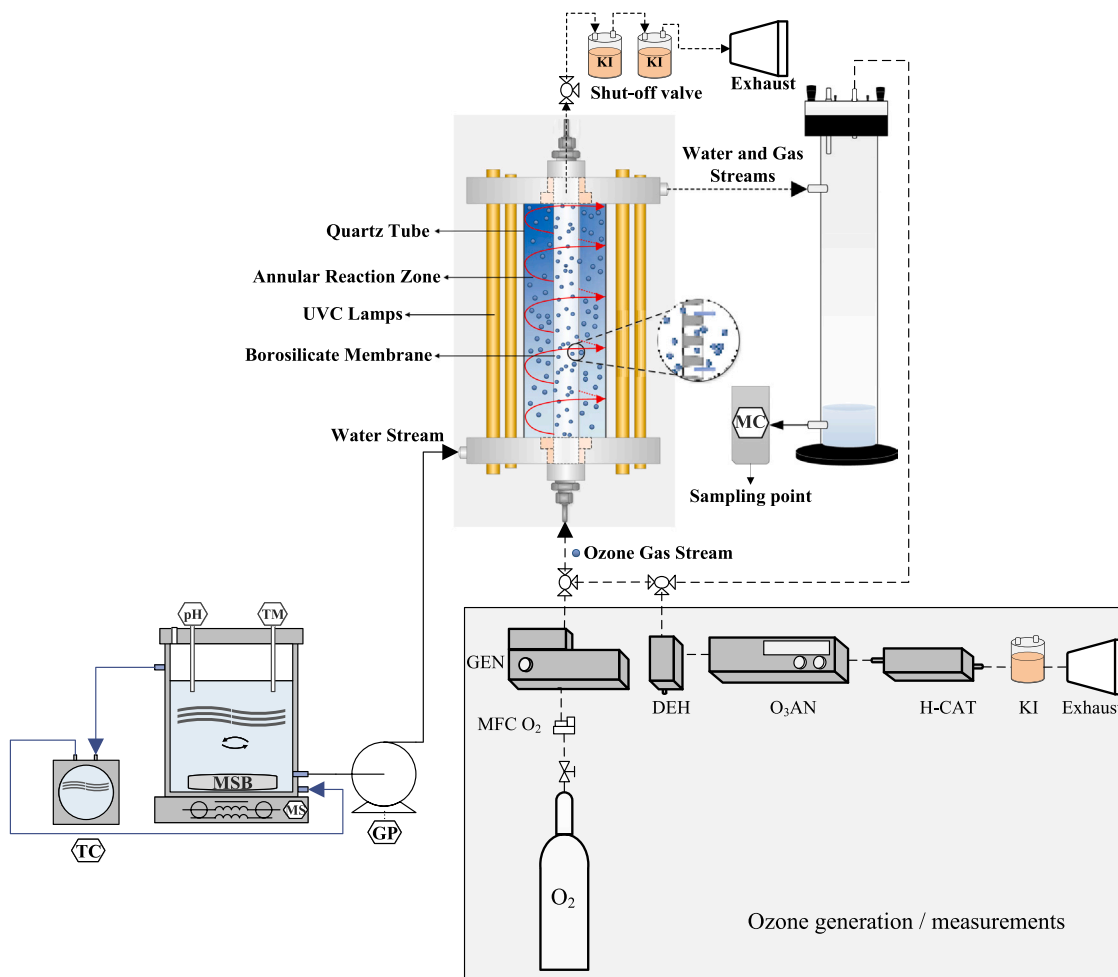

Fig. 1. Schematic representation of laboratory-scale setup. Note: DEH – dehumidifier; GEN – ozone generator; GP – gear pump; H-CAT – heat catalyst (ozone destruction); MC – ozone measuring cells; MFC – mass flow controller; MS – magnetic stirrer; MSB – magnetic stir bar; O_2 – oxygen; O_3AN – ozone analyser; pH – pH-meter; TC – temperature controller; TM – temperature meter; Continuous lines – water; Dotted lines – water + ozone gas stream; Dashed lines – ozone gas stream.

specifications, the measuring range was 0.05–50 g O_3 m^{-3}, sensitivity < 0.02 g O_3 m^{-3}, and accuracy < ± 5%. The O_3 probe was calibrated using the iodometric method, based on the oxidation of iodide with O_3 and posterior evaluation of the produced iodine or its ion in solution [21,22]. The analysis of iodine was made by titration with $Na_2S_2O_3$. The iodometric method is described in detail in the Supplementary Information.

2.2.2. Ozone membrane reactor

The ozone membrane reactor comprises an inner tubular borosilicate microfiltration membrane (ASTM VitraPOR from ROBU; outside diameter: 20.9 mm; internal diameter: 10.5 mm; wall thickness: 5.2 mm; useful length: 174 mm; porosity: 45%; BET: 1200 m^2 g^{-1}) with 5 μm pore size adequately installed in an outer quartz tube (outside diameter: 42.2 mm; internal diameter: 38.2 mm; length: 200 mm) vertically fixed in a stainless-steel structure. The borosilicate membrane and quartz tube ends were tightly sealed by two movable polypropylene flanges. The membrane outlet was connected to a shut-off valve to allow gas permeation through the porous glass membrane. In this system, the O_3 gas stream is fed by the lumen side of the membrane, while the water to be treated is introduced in the shell side of the membrane, and the gas/water contact takes place at the outer membrane surface. DW (with or without CECs) was pumped from a jacketed vessel to the ARZ using a gear pump (ISMATEC BVP-Z pump). Viton O-rings (ozone-resistant) were used to ensure sealing conditions within the reaction module. Polytetrafluoroethylene (PTFE) and stainless-steel tubes were used to connect the liquid and gas units of the system, respectively.

To assess the effect of combining the ozonation process with photocatalysis in the removal of CECs, four UVC lamps (Philips TL 11 W, $\lambda_{max} = 254$ nm) were located externally to the reactor window. UVC radiation was chosen since it is able to effectively activate both TiO_2 and O_3. O_3 has an absorption band at 200–300 nm with a maximum at λ of 254 nm [23,24]). A photon flow (2.89 ± 0.08 W) inside the ARZ was measured by ferrioxalate actinometry [25,26] ($Fe^{3+} = 6 \times 10^{-3}$ M; overall quantum yield, $\Phi_T = 1.39 \pm 0.02$; optical path length = 8.65 mm;). An aluminium shell enclosed the illuminated reactor setup to prevent light escape to the surroundings.

2.3. Photocatalytic borosilicate membrane

2.3.1. Preparation of the photocatalytic membrane

The membrane was first cleaned with a 10% HCl solution and ultrapure water according to the procedure recommended by the manufacturer. 2% (w/v) TiO_2-P25 suspension (250 mL) with two drops of TritonTM X-100 was stirred for 24 h and placed in an ultrasonic probe (Vibra-Cell™ VCX 130 from Sonics) with a frequency of 20 kHz (80% amplitude) for 15 min. The prepared suspension was used to coat the external surface of the membrane following an immersion coating method [27], employing an automatic dip-coating unit (RDC 15 from Bungard-Elektronik) with an immersion rate of 8 cm min^{-1} and immersion time of 1 min. After each immersion, the membrane was dried in an oven at 100 °C for 15 min. The process was repeated four times and, afterwards, the membrane decorated with TiO_2-P25 was taken for heat treatment in a furnace (up to 450 °C for 2 h). Before its use in photocatalytic tests, the coated membrane was placed inside the reactor and ultrapure water was recirculated throughout the system in the dark for 1 h to remove unbounded TiO_2-P25 particles. The total mass of catalyst deposited on the membrane was calculated by weighing the membrane before catalyst deposition and after the cleaning and drying process.

2.3.2. Characterization of the photocatalytic membrane

The membrane surface morphology was observed by scanning electron microscopy (SEM). A Jeol JSM 7401 F Field Emission Scanning Electron Microscope equipped with Gentle Beam mode was employed to characterise the developed modified membranes' surface morphology.

X-ray powder diffraction (XRD) patterns of the samples that performed the phase identification were recorded on a D/max 2550Pc automatic diffractometer of polycrystalline (Cu Kα radiation, Rigaku-D/MAX2500/PC, Japan) that operated at 40 keV and 100 mA over the range of 20 ° < 2θ < 90 ° at a scanning rate of 0.02°s^{-1}. Mercury intrusion porosimeter equipment (PoreMaster 60, Quantachrome Inst.) was used to determine the pore size and porosity of the membrane after TiO_2-P25 deposition.

2.4. Evaluation of gas/liquid mass transfer

Ozone gas/water mass transfer was determined in continuous mode operation and the effect of water pH and temperature (T), the concentration of O_3 in the gas stream ([O_3]$_G$), liquid (Q_L) and gas (Q_G) flow rates in the volumetric mass transfer coefficient (K_La) was assessed. Table 1 presents the experimental conditions used in all gas/liquid mass transfer tests. To begin the experimental trial, the borosilicate membrane was filled internally with the ozone gas stream with the shut-off valve fully open (Fig. 1). This procedure ensured that the entire interior of the membrane was filled with the gas. The residual O_3 stream was directed to a 2% KI solution in an O_3 destroyer bottle. Subsequently, DW was pumped and the shut-off valve was immediately closed. The concentration of dissolved O_3 in the water at the reactor outlet was analysed in situ, and the data were collected at regular time intervals.

2.4.1. Gas/liquid mass transfer calculations

The two-film theory was used for the modeling of the O_3 mass transfer, typically controlled by resistance on the liquid side. As O_3 is slightly soluble in water, resistance to mass transfer is located in the liquid film [28]. Thus, the volumetric mass transfer coefficient (K_La) can be calculated from the mass balance of O_3 in the liquid, considering plug flow conditions, and represented by Eq. 1:

$$\frac{d[O_3]}{dt} = K_La \times ([O_3^*] - [O_3]) - k_d[O_3] \tag{1}$$

Where, $\frac{d[O_3]}{dt}$ is the variation of dissolved O_3 concentration in water as a function of time (mg L^{-1} min^{-1}), K_La is the product of the O_3 mass transfer coefficient (min^{-1}) through the liquid phase (K_L) and the interfacial area (a), [O_3]* is the O_3 saturation concentration in the liquid in equilibrium with the gas phase (mg L^{-1}) at the experimental temperature and k_d is the self-decomposition constant of O_3.

The self-decomposition of O_3 ($k_d = (131 \pm 7) \times 10^{-4}$ min^{-1}) is a very slow step when compared to the O_3 dissolution process (see supplementary data file). Therefore, considering a negligible self-decomposition constant of O_3 and the following boundary conditions for continuous mode operation: [O_3] = 0 at t = 0; [O_3] = [O_3]$_L$ at t = τ, the integration of the Eq. (1) leads to Eq. (2):

$$K_La = -\frac{1}{\tau} \times \ln \left(1 - \frac{[O_3]_L}{[O_3^*]}\right) \tag{2}$$

where [O_3]$_L$ is the dissolved ozone concentration in the outlet liquid stream at steady-state conditions, and τ is the liquid residence time, calculated taking into account the gas holdup (ε_G).

The parameter a is essential for processes involving gas-liquid mass transfer (Eq. 3) and requires the determination of ε_G and the Sauter mean diameter (d_{32}), which can be obtained from the bubble size distribution data (Eq. 4).

$$a = 6 \times \frac{\varepsilon_G}{d_{32}} \tag{3}$$

$$d_{32} = \frac{\sum_{i=1}^{n} n_i \times d_{eq}^3}{\sum_{i=1}^{n} n_i \times d_{eq}^2} \tag{4}$$

where n_i is the number of bubbles of diameter d_{eq}.

Table 1
Experimental conditions employed in all ozone mass transfer tests.

Q_G (Ndm^3 min^{-1})	$[O_3]_G$ (g Nm^{-3})	Q_L (L h^{-1})	τ (s)	pH	Temperature (ºC)	$[O_3^*]$[a] (g m^{-3})	$[O_3]_L$[a] (g m^{-3})	K_La[a] (min^{-1})
Effect of pH								
0.75	21.0	50	10.1	3.28	20	4.65 ± 0.07	3.18 ± 0.05	6.86 ± 0.03
0.75	21.6	50	10.1	5.00	20	3.02 ± 0.02	1.86 ± 0.01	5.70 ± 0.08
0.75	20.8	50	10.1	6.96	20	2.55 ± 0.01	1.39 ± 0.01	4.69 ± 0.07
0.75	20.6	50	10.1	9.00	20	1.16 ± 0.05	0.58 ± 0.02	4.13 ± 0.04
Effect of Temperature								
0.75	21.4	50	10.1	3.28	15	4.8 ± 0.1	3.54 ± 0.04	8.02 ± 0.08
0.75	21.0	50	10.1	3.28	20	4.65 ± 0.07	3.18 ± 0.05	6.86 ± 0.03
0.75	21.2	50	10.1	3.29	25	4.5 ± 0.1	3.02 ± 0.03	6.59 ± 0.05
Effect of Q_L								
0.75	20.3	20	25.2	3.28	20	4.65 ± 0.07	3.57 ± 0.04	3.51 ± 0.01
0.75	20.3	30	16.8	3.21	20	4.65 ± 0.07	3.42 ± 0.03	4.79 ± 0.02
0.75	20.1	35	14.4	3.14	20	4.65 ± 0.07	3.28 ± 0.09	5.13 ± 0.03
0.75	20.0	40	12.6	3.24	20	4.65 ± 0.07	3.20 ± 0.04	5.59 ± 0.05
0.75	21.0	50	10.1	3.28	20	4.65 ± 0.07	3.18 ± 0.05	6.86 ± 0.03
0.75	20.0	60	8.4	3.20	20	4.65 ± 0.07	2.81 ± 0.07	6.83 ± 0.02
0.75	20.1	150	3.4	3.12	20	4.65 ± 0.07	1.36 ± 0.02	6.18 ± 0.06
Effect of $[O_3]_G$								
0.75	21.0	50	10.1	3.28	20	4.65 ± 0.07	3.18 ± 0.05	6.86 ± 0.03
0.75	40.0	50	10.1	3.20	20	11.15 ± 0.06	8.06 ± 0.07	7.64 ± 0.02
0.75	60.3	50	10.1	3.14	20	21.14 ± 0.08	14.8 ± 0.1	7.12 ± 0.08
0.75	80.3	50	10.1	3.08	20	30.7 ± 0.2	22.3 ± 0.1	7.7 ± 0.2
Effect of Q_G								
0.15	80.8	50	10.1	3.21	20	30.7 ± 0.2	19.3 ± 0.2	5.9 ± 0.1
0.30	81.8	50	10.1	3.17	20	30.7 ± 0.2	19.7 ± 0.2	6.1 ± 0.1
0.50	80.0	50	10.1	3.09	20	30.7 ± 0.2	21.2 ± 0.9	7.0 ± 0.2
0.75	80.3	50	10.1	3.08	20	30.7 ± 0.2	22.3 ± 0.1	7.7 ± 0.2
0.75	21.0	50	10.1	3.28	20	4.65 ± 0.07	3.18 ± 0.05	6.86 ± 0.03
0.85	23.0	50	10.1	3.30	20	4.65 ± 0.07	3.45 ± 0.03	8.1 ± 0.7
1.00	22.0	50	10.1	2.90	20	4.65 ± 0.07	3.63 ± 0.04	9.0 ± 0.4

[a] Standard Error

Images obtained from a high-speed digital video camera (Photron, FASTCAM SA-Z) allowed the determination of the bubble size distribution and mean bubble size. Further details are provided in Supplementary Information.

In O_3 membrane contactors, the membrane creates an additional mass transfer resistance, significantly reducing process efficiency. For a conventional membrane contactor with a hydrophilic membrane, the overall mass transfer resistance ($1/K_L$) is given by Eq. (5) [29].

$$\frac{1}{K_L} = \frac{1}{k_G H} + \frac{1}{k_M} + \frac{1}{k_L} \tag{5}$$

where k_G, k_M, and k_L are the individual mass transfer coefficients for the gaseous phase, the membrane, and the liquid phase, respectively; $1/k_G H$, $1/k_M$ and $1/k_L$ are the mass transfer resistances in the gas boundary layer, membrane matrix, and liquid boundary layer, respectively; H is the Henry coefficient. In a gas-liquid membrane contactor, the resistance to mass transfer in the liquid boundary layer has already been proved to be the dominant step of overall mass transfer resistance for the case of low liquid Reynolds number and low gas solubility [30]. As a result, the simpler model can be obtained when the mass transfer resistance in the gas phase is neglected (i.e., $1/k_G H \cong 0$), owing to the ozone diffusion coefficient in the gas phase is 4 orders of magnitude higher than in the water [31,32] (Eq. 6).

$$\frac{1}{K_L} = \frac{1}{k_M} + \frac{1}{k_L} \tag{6}$$

2.5. Evaluation of CECs removal

CECs removal was evaluated in continuous mode using DW contaminated with 19 CECs (10 μg L^{-1} each) and different reaction processes: (i) ozonation (with O_3 permeation and light irradiation off); (ii) photocatalysis UVC/TiO$_2$ (no O_3 permeation), and (iii) photocatalytic ozonation (O_3/UVC/TiO$_2$). The following operational conditions were applied: CECs solution inlet flow rate ($Q_L = 150$ L h^{-1}), O_3 concentration at the gas inlet ($[O_3]_G = 5, 20, 40, 60, 100$ or 200 g Nm^{-3}), and gas flow ($Q_G = 0.15$ or 0.75 Ndm^3 min^{-1}), corresponding to different inlet O_3 doses ($OD_I = 2, 6, 12$ or 18 g m^{-3}). The ozone concentrations in the inlet and outlet of the system were monitored and the transferred ozone dose (TOD; g m^{-3}) was calculated according to Eq. 7:

$$TOD = \frac{([O_3]_G - [O_3]_{Gout}) \times Q_G}{Q_L} \tag{7}$$

where $[O_3]_{Gout}$ is the O_3 concentration in the outlet gas stream.

The samples were taken at pre-determined time intervals and the residual ozone was removed immediately by placing the samples in a water bath at 80 ºC. After each experiment, the ozone membrane contactor was washed by pumping DW through the ARZ.

2.5.1. CECs analysis

The analysis of the selected CECs in water samples was performed in an Acquity UPLC® liquid chromatograph interfaced to a XEVO TQD® triple quadrupole mass spectrometer (LC-MS/MS) equipped with an electrospray interface (ESI) from Waters (Milford, MA, USA). The analytical methodology is described in detail in the Supplementary Information, including Table S2 and Table S3.

3. Results and discussion

3.1. Characterisation of TiO$_2$ coated borosilicate membrane

The membrane prior to and after catalyst immobilization was examined using the SEM technique (Fig. 2). The fresh borosilicate surface (Fig. 2a) is typical of a silica-based material with the presence of nanoparticles and significant roughness. On the other hand, the surface of the membrane with TiO$_2$-P25 composite (Fig. 2b) became more uniform and presented fewer imperfections and roughness compared to the unmodified membrane. Uniform deposition of c.a. 623 mg of TiO$_2$-P25 over the entire membrane was obtained after 4 immersions in the
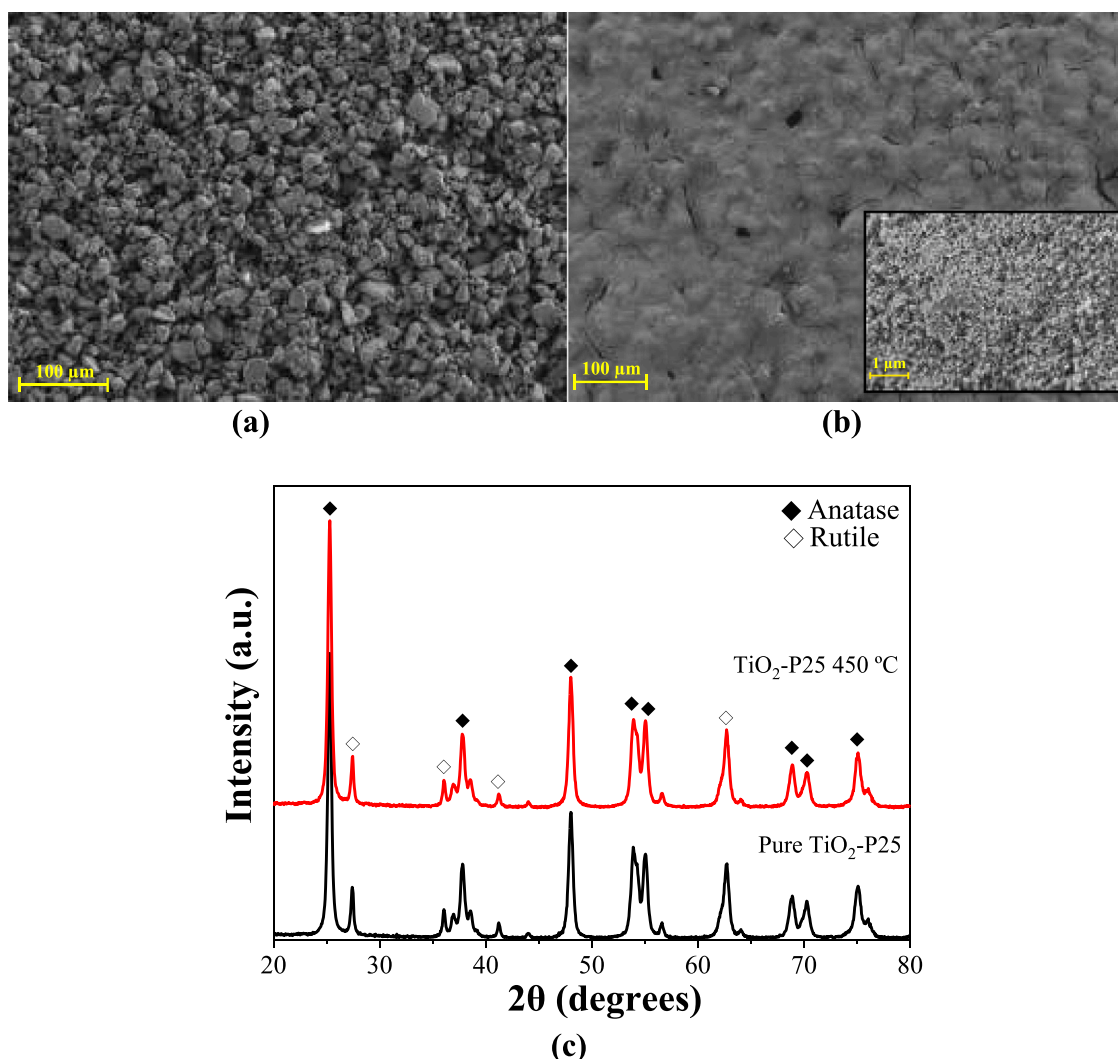
Fig. 2. SEM images of the (a) unmodified borosilicate membrane, (b) borosilicate membrane after deposition of TiO_2-P25 (2% w/v), and (c) XDR patterns of pure TiO_2-P25 and after thermal treatment.

catalyst suspension, which allowed not only the occurrence of thin-films of the catalyst on the membrane surface, but also an accumulation of large amounts of TiO_2-P25 particles in the membrane pores (not attained with fewer immersions). Consequently, after the addition of the TiO_2 surface layer, the membrane showed a pore size of 3.8 μm, meaning a decrease in the initial pore size of the pristine membrane (5 μm). This allows reducing the size of the O_3 bubbles generated by the contact between the membrane surface and the liquid phase. In this case, an average size of 0.20 ± 0.04 mm of O_3 bubbles was obtained, with $> 60\%$ of bubbles < 0.1 mm, followed by $> 30\%$ of bubbles between 0.1 and 0.3 mm (Conditions: $Q_L = 150$ L h^{-1}; $Q_G = 0.75$ Ndm^3 min^{-1}; T = 20 °C). More details on the bubble size measuring are reported in Supplementary Information. The average bubble diameter for bubble column can vary between 2 and 4 mm [33].

TiO_2-P25 films deposited on the membrane surface were subjected to thermal treatment (at 450 °C) to stabilize the catalyst on the membrane surface. The XRD pattern of the material before and after thermal treatment (Fig. 2c) confirmed a mixed anatase crystal structure (JCPDS file No.73–1764) and rutile crystal structure (JCPDS file No.78–1510). The distinct diffraction peaks observed in the 2θ values of 25.3 °, 37.8 °, 48.0 °, 54.0 °, 55.1 °, 68.9 °, 70.3 °, and 75.0 ° correspond to (101), (004), (200), (211), (105), (204), (116), (220) and (215) of the anatase crystal planes. The distinct diffraction peaks for rutile are observed at 27.5 °, 36.1 °, and 41.3 °, corresponding to the (110), (101), and (111) planes,

respectively. Consequently, the expected photocatalytic activity of the TiO_2-450°C immobilised on the membrane surface is very similar to TiO_2-P25.

3.2. Effect of operating parameters on K_La in the ozone membrane contactor

3.2.1. Water pH and temperature

The increase in the water pH (from 3 to 9) negatively influenced K_La values (Table 1 and Fig. 3), as reported by Roth and Sullivan [34], who point to a decrease in Henry's constant for O_3 in water as the pH drops. According to the authors, a lower value of Henry's constant leads to a higher value of solubility and, consequently, of K_La. Thus, the concentration of O_3 in water ([O_3]$_L$) increased gradually as the pH dropped (Table 1 and Fig. 3), with [O_3]$_L$ at pH 3 around 3 times higher than at pH 7. Decreasing the pH of the solution can help reduce O_3 self-decomposition (since hydroxide ions act as reaction initiators, Eqs. 8 and 9 [35–37]) and promote the dissolution of O_3 in the liquid phase. Therefore, for better gas-liquid mass transfer results and increased O_3 concentration in the water, the pH of the solution must be reduced to create an acidic environment minimising the presence of hydroxide ions. Thus, to avoid the decomposition of the molecular ozone into hydroxyl radicals, all the tests to assess mass transfer were carried out at a pH value of 3.
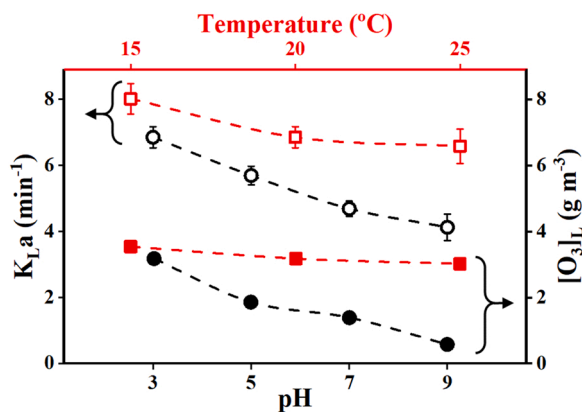
Fig. 3. Effect of water pH value (— ○ —; — ● —) and operating temperature (— □ —; — ■ —) on K_La value (open symbols) and on ozone solubility in the liquid-phase-$[O_3]_L$ (closed symbols). Conditions: $Q_L = 50$ L h^{-1}; $[O_3]_G = 20$ g Nm^{-3}; $Q_G = 0.75$ Ndm^3 min^{-1}.

$$O_3 + OH^- \rightarrow HO_2^- + O_2 \qquad (8)$$

$$O_3 + HO_2^- \rightarrow OH^\bullet + \quad O_2 + O_2^- \qquad (9)$$

According to Henry's law, the solubility and half-life of the O_3 molecule can be directly affected by the liquid temperature. The water temperature was shown to be inversely proportional to the O_3 concentration in the liquid-phase (Table 1 and Fig. 3). Therefore, by increasing

the temperature: (i) the O_3 decomposition was accelerated and the stability of O_3 in water decreased, thus reducing the $[O_3]_L$ [38]; (ii) specific properties of the liquid were changed, such as lower surface tension and viscosity, increasing the transfer resistance through the liquid-phase due to the reduction of cavitation intensity [39]. As can be seen in Fig. 3, the K_La value reached a maximum reduction of approximately 20% at a 10 °C increase in temperature (15 °C to 25 °C) and the amount of O_3 in the water showed a small tendency to fall with the increase of the operational temperature (Fig. 3). The small difference in the K_La value between 20 °C and 25 °C may be related to the fact that this parameter involves two opposite contributions. On the one hand, Henry's constant decreases as the temperature increases, leading to lower O_3 solubility. On the other hand, the Arrhenius equation predicts an increase in the reaction rate of ozonation with temperature [40]. Despite this, ozonation has the advantage of taking place under normal conditions of temperature, thus minimising the need to heat the reactor, which is economically preferable. Thus, hereafter only data taken at 20 °C will be analysed.

3.2.2. Liquid flow rate

For different liquid flow rates ($Q_L = 20$–150 L h^{-1}), it can be seen (Fig. 4a) that the K_La value increased up to Q_L of 50 L h^{-1} and after that remained constant. A possible reason for this phenomenon is that with increasing Q_L there is a more significant liquid turbulence, i.e., a higher Reynolds number, resulting in the formation of smaller gas bubbles or thinner liquid films, with a consequent increase in the interfacial area, and reducing the resistance to O_3 transfer in the water phase boundary layer. Furthermore, hydrodynamics studies of tubular photoreactors
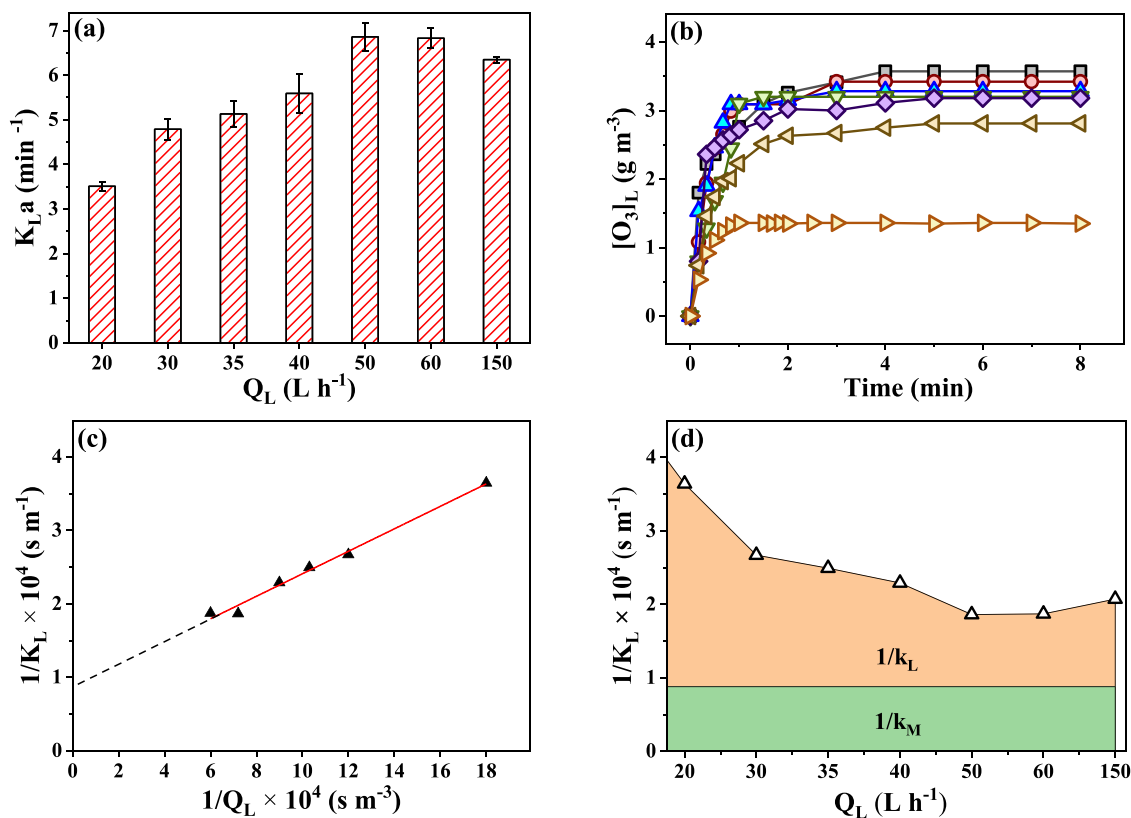

Fig. 4. Effect of liquid flow rates (a) on K_La value and (b) on dissolved ozone concentration over time; (c) "Wilson plots" for volumetric mass transfer coefficient and water flow, and (d) mass transfer resistances in the water phase boundary layer ($1/k_L$) and in the membrane ($1/k_M$) as a function of water flow rate ($Q_L = 20$ (—■—), 30 (—○—); 35 (—▲—); 40 (—▽—); 50 (—◆—); 60 (—◀—); 150 (—▷—) L h^{-1}). Conditions: $Q_G = 0.75$ Ndm^3 min^{-1}; $[O_3]_G = 20$ g Nm^{-3}; T = 20 °C; pH = 3.

with tangential position of inlet/outlet pipes have shown that these reactors tend to exhibit turbulent flow patterns even at low Reynolds numbers [41] and a longer effective flow path (i.e., longer contact time) due to the helical motion of the water around the inner tube [20]. Another reason for this phenomenon is that the shear rate on the membrane surface increases as the flow rate increases. Therefore, the microbubbles attached by surface tension to the membrane surface are removed faster. It is worth remembering that when the reactor works in continuous mode, there is a direct interference between the liquid velocity and the residence time. Therefore, with the increase in the liquid flow, inversely occurs the reduction of the concentration of O_3 in the water at steady-state (Fig. 4b). Thus, the $[O_3]_L$ decreased from 3.6 g m^{-3} to 1.4 g m^{-3} when Q_L increased from 20 L h^{-1} to 150 L h^{-1}.

The membrane mass transfer coefficient (k_M) was obtained from "Wilson plot", whereby the values of $1/K_L$ was plotted against $1/Q_L$ (Fig. 4c). Thus, the mass transfer resistance in the membrane ($1/k_M$) was determined by extrapolating the linear fit of the data to $1/Q_L = 0$, implying $Q_L \rightarrow \infty$ and thus $1/k_L \approx 0$ (see Eq. 6). The same linear trend has been reported in other studies combining membranes with O_3 [29] and O_2 [42]. A least-squares regression analysis of the data in Fig. 4c gave a value of $1/k_M = (8.8 \pm 0.1) \times 10^3$ s m^{-1} for the tubular porous borosilicate membrane, which corresponds to the k_M value of $(1.14 \pm 0.01) \times 10^{-4}$ m s^{-1}. The resistance in the membrane matrix is affected by pore size, membrane thickness and hydrophobicity. Membranes with smaller pores, larger thicknesses and lower hydrophobicity present greater resistance to O_3 mass transfer [43]. This emphasizes the importance of the structural material used. The mass transfer coefficient in the membrane can be also calculated from the structural properties of the membrane as [42]:

$$k_M = \frac{D_M \times \varepsilon}{\tau_p \times \Delta x} \qquad (10)$$

where D_M is the effective diffusion coefficient of ozone in the membrane (m^2 s^{-1}), ε is the porosity of the membrane (45%), τ_p is the pore tortuosity and Δx is the membrane thickness (5.2 mm). The τ_p was estimated by the porosity-tortuosity relationship defined by Iversen et al. [44] ($\tau_p = (2 - \varepsilon)^2/\varepsilon$). Inside the membrane pores, the gas can flow by molecular diffusion and Knudsen diffusion. D_M can therefore be expressed as Eq. 11 [45]:

$$D_M = \frac{1}{\frac{1}{D_{O_3}} + \frac{1}{D_K}} = \frac{1}{\frac{1}{D_{O_3}} + \frac{1}{\frac{d_{pore}}{3} \times \sqrt{\frac{8}{\pi} \times \frac{R \times T}{\times M}}}} \qquad (11)$$

where D_K is the Knudsen diffusion coefficient, defined by $D_K = \frac{d_{pore}}{3} \times \sqrt{\frac{8 \times R \times T}{\pi \times M}}$, D_{O3} is the diffusion coefficient of ozone in the gas phase (2×10^{-5} m^2 s^{-1} at 20 °C [32]), T is the temperature (293.15 K), M is the molar mass of ozone (47.998 g mol^{-1}), R is the ideal gas constant (8.3145 J K^{-1} mol^{-1}), and d_{pore} is the mean pore diameter (3.8×10^{-6} m). By substituting the terms in Eq. 10 gives $k_M = 1.4 \times 10^{-4}$ m s^{-1} which is slightly higher than the experimental k_M value of $(1.14 \pm 0.01) \times 10^{-4}$ m s^{-1}. This shows the consistency of the experimental results obtained. Moreover, using Eq. 6 and the experimental values K_L and k_M, the liquid-phase mass transfer coefficient (k_L) can be obtained by the following equation (Eq. 12).

$$k_L = \left(\frac{1}{K_L} - \frac{1}{k_M} \right)^{-1} \qquad (12)$$

The results of individual mass-transfer resistances for O_3 dissolution in water are shown in Fig. 4d. The resistance to diffusion through the water phase boundary layer ($1/k_L$) is the main resistance to ozone transfer providing 53–76% of the total mass transfer resistance, while the contribution of the membrane phase varies between 24% and 47%. In the present study, the membrane was doped with TiO_2, which has a superhydrophilic character. Kukuzaki et al. [29] reported the main

resistances to ozone transfer for hydrophilic and hydrophobic membranes and showed that the individual mass transfer coefficient for membrane and water phase were higher when using a hydrophobic membrane. This is a consequence of the liquid penetration into the pores which over time makes the resistance in the membrane more significant and closer to the liquid phase resistance [46]. Hence, it is assumed that the membrane pores were partially wetted, leading to a higher membrane resistance than the non-wetted pores. The reduction in resistance to diffusion through the water phase boundary as flow rate increased (Fig. 4d) resulted from higher shear over the membrane, which favoured faster removal of the microbubbles attached by surface tension to the membrane surface.

3.2.3. Applied ozone concentration

The effect of O_3 concentration in the inlet gas stream ($[O_3]_G$) on the values of $[O_3]_L$ and on $K_L a$ are summarised in Table 1 and Fig. 5. Note that when $[O_3]_G$ increases 4 times (from 20 g Nm^{-3} to 80 g Nm^{-3}), $[O_3]_L$ raises ~7 times (from 3.18 g m^{-3} to 22.3 g m^{-3}) (Fig. 5a). The relationship between O_3 in the gas-phase and soluble O_3 in the liquid-phase can be represented by Henry's law. The concentration of dissolved O_3 in water at steady-state increases with the enhancement of equilibrium pressure and O_3 gas concentration, due to the higher O_3 diffusion rate [29]. Therefore, by increasing the $[O_3]_G$, more O_3 molecules are available in the liquid-phase, improving O_3 concentration (driving force). In turn, the $K_L a$ values for the different initial $[O_3]_G$ were almost constant and independent (Fig. 5b), which shows the stability of the ozone mass transfer device in good agreement with those observed by other studies [29,47,48]. The rate of mass transfer is obviously controlled by the degree of turbulence and shear in the shell side of the membrane.

3.2.4. Inlet ozone gas flow rate

The mass transfer results (Fig. 6) indicate that a higher ozone gas flow rate (Q_G) decreases the required time to reach the dissolved O_3 equilibrium in the reactor and slightly improves the equilibrium concentration. With the increase in Q_G, the amount of O_3 injected per unit of time increases and, thereby, accelerates the dissolution rate of O_3 until equilibrium (Fig. 6a). Additionally, an increase in the gas flow rate enhances the turbulence in the gas-liquid interface [29] and, therefore, improve the number/velocity of the generated bubbles and disperse the liquid better, resulting in a higher gas-liquid interface area and enabling a higher mass transfer (Fig. 6b). Moreover, the liquid is fed tangentially to the inner surface of the outer tube, inducing a helical motion of the water that provides additional gas mixing. It reduces local points near the external membrane surface where greater O_3 concentrations are observed, enhancing the mass transfer. A pressure differential between
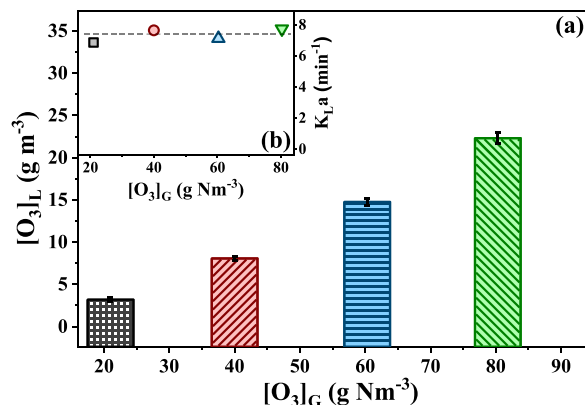

Fig. 5. Effect of applied ozone concentration on ozone solubility in the liquid-phase (a) for ozone concentrations of 20 (▦), 40 ▨, 60 ▤ and 80 ▨ g Nm^{-3} and (b) the respective $K_L a$ values. Conditions: Q_L = 50 L h^{-1}; Q_G = 0.75 Ndm^3 min^{-1}; T = 20 °C; pH = 3.
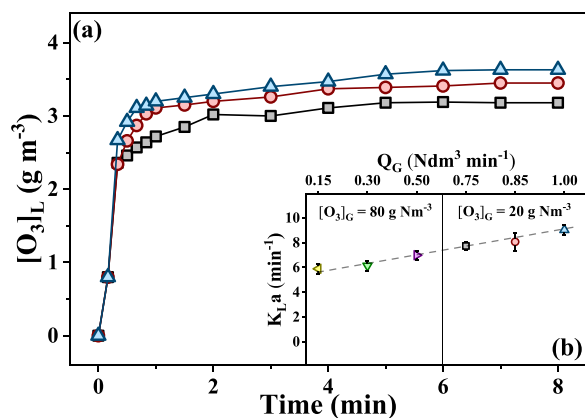
Fig. 6. Effect of inlet ozone gas flow rate (a) on ozone solubility in the liquid-phase for gas flow of 0.75 ▬□▬, 0.85 ▬○▬ and 1.00 ▬△▬ Ndm^{-3} min^{-1} and (b) in the respective $K_L a$ values. Conditions: $Q_L = 50$ L h^{-1}; $[O_3]_G = 20$ g Nm^{-3}; T = 20ºC; pH = 3.

the gas and water phases can enable larger O$_3$ dosages and control the amount of O$_3$ delivered to the water.

In continuous mode, raising the gas velocity from 0.75 to 1.00 Ndm^3 min^{-1}, $K_L a$ increased 1.3-fold, presenting its highest value in DW with no reaction (9.0 ± 0.4 min^{-1}, Table 1). Considering that in conventional ozonation processes, $K_L a \cong k_L a$, the intensified volumetric mass transfer coefficients obtained in this work is higher than in bubble columns [49] and comparable to a highly optimized venturi injectors [50] and static mixers [51] (Table 2). Moreover, membrane contactors have further advantages over conventional injectors. Membrane length can be quickly increased, meaning even more O$_3$ "dosing" points, which is not possible for conventional single-point injection systems, like the venturi tube and static mixer. In addition, functionalized membranes can be applied to enhance the performance of the ozonation system, either for O$_3$/O$_2$ separation to obtain an O$_3$-enriched gas stream or for promoting synergetic catalytic effects with O$_3$. Compared with other membrane contactors (Table 2), the present study enabled higher mass transfer coefficients ($K_L a$ and K_L - from 2 to 30 times higher, except for the study of Pines et al. [52]), as allows the use of functionalised membrane to promote synergistic effects between photocatalysis and ozonation for water/wastewater treatment purposes.

3.3. Mass transfer efficiency (MTE)

The mass transfer efficiency (MTE) is defined as the portion of applied O$_3$ that goes into the solution and is calculated from the mass of applied O$_3$ and the mass of O$_3$ in the liquid-phase as follows (Eq. 13):

$$MTE(\%) = \frac{Q_L \times [O_3]_L}{Q_G \times [O_3]_G} \times 100 \tag{13}$$

For a fixed Q_L of 50 L h^{-1} (Fig. 7), a slight increase on MTE was

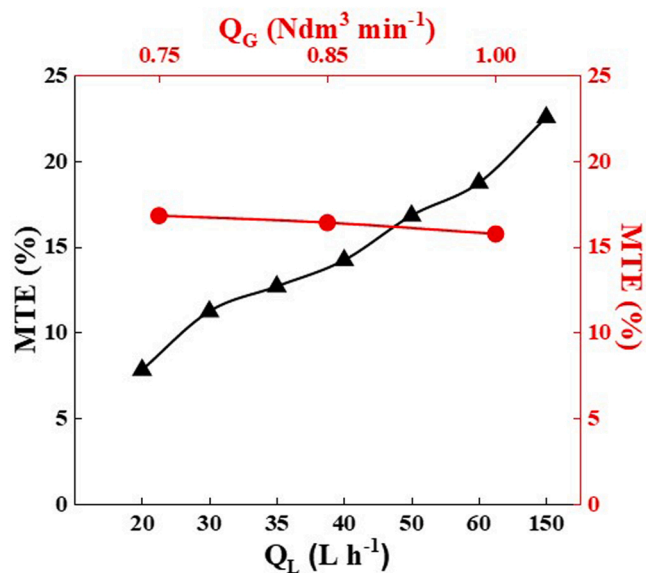**Fig. 7.** Ozone mass transfer efficiency (MTE %) as a function of water ▬▲▬ and inlet gas ▬●▬ flow rates obtained using the ozone membrane contactor. Conditions: $[O_3]_G = 20$ g Nm^{-3}; T = 20 ºC; pH = 3; fixed $Q_L = 50$ L h^{-1} or fixed $Q_G = 0.75$ Ndm^3 min^{-1}.

observed with the decrease in the Q_G, mainly associated with a higher contact time between both phases. On the other hand, for a fixed Q_G of 0.75 Ndm^3 min^{-1}, it can be seen that the MTE increased proportionally with the water flow (Fig. 7). This indicates the ability to work with low gas/liquid volumetric ratios, which is an appealing feature when considering the treatment of large volumes of wastewaters, such as secondary effluents from urban wastewater treatment plants (WWTPs). For the operational conditions tested, the highest mass transfer efficiency of 23% was obtained by applying the lowest input Q_G, 0.75 Ndm^3 min^{-1}, and the highest Q_L, 150 L h^{-1}. Other contacting devices such as multi-orifice oscillatory baffled column can achieve higher rates of MTE although the equipment involved may require higher power input [53]. Therefore, these conditions were selected for the following ozonation tests to assess the membrane contactor application for the removal of a mixture of CECs in water.

3.4. Ozone membrane contactor for the degradation of CECs

The effectiveness of the ozone membrane contactor was evaluated by targeting the removal of 19 CECs in deionized water at natural pH of 6.5. The target CECs include four short-chain perfluorinated compounds (HFBA, PFBS, PFOA, TFMS), three angiotensin II receptor blockers (VSTN, ISTN, LSTN), two beta-blockers (ATNL and BSPL), two hormones (E2 and EE2), an anti-inflammatory (DCF), two artificial sweeteners (AC-K and SCH), a flame retardant (MLN), an herbicide (DRN), an insect

Table 2
Characteristics of ozone-liquid contacting systems.

Type of contactor		Liquid flow (L h^{-1})	Gas flow (Ndm^3 min^{-1})	$K_L a$ (min^{-1}) / K_L (m s^{-1})	Reference
Conventional	Static mixers	90–138	0.4–0.8	6–18 min^{-1}	[51]
	Venturi injectors	1080–6336	3–24	4.2–18 min^{-1}	[50]
	Bubble column	100–450	5–20	0.18–1.2 min^{-1}	[49]
Membrane	Non-porous tubular polydimethylsiloxane (PDMS)	0.3–1.2	0.1	2.4 × 10^{-6} m s^{-1}	[70]
	Tubular Shirasu porous glass (SPG)	72–480	0.2	1.2 × 10^{-5} m s^{-1}	[29]
	Polytetrafluorethylene (PTFE) hollow fiber membrane	100–500	–	0.438 min^{-1}	[39]
	Flat porous and non-porous Teflon membranes	1.5–120	0.10–0.11	7.6 × 10^{-5} m s^{-1}	[52]
	Polytetrafluoroethylene (PTFE) hollow fiber membrane	100–500	–	0.7858 min^{-1}	[71]
	Tubular porous borosilicate	20–150	0.15–1.00	3.5–9.0 min^{-1} / 5.4 × 10^{-5} m s^{-1}	This work

repellent (DEET), carbamazepine (CBZ) and its metabolite (CBZ-EPX). These CECs were selected based on their occurrence in the water cycle, persistence during treatment and potential toxicity to health and the environment, according to the results obtained in several screening campaigns conducted under the NOR-WATER project (http://nor-water. eu/en/home/). CECs in water can react simultaneously with ozone (direct reaction) and hydroxyl radicals (indirect reaction) at different rates depending on the water pH. The underlying mechanisms for in situ formation of hydroxyl radicals by oxidation of water with O_3 at pH 7–9 have been extensively described in the literature [32,35,54,55].

As shown in Fig. 8a, the ozonation showed satisfactory degradation (>80% for 13 out of the 19 CECs) applying an ozone dose of 12 g m^{-3} (TOD = 4.3 g m^{-3}) and a Q_L of 150 L h^{-1}. The greater removal of CECs as a function of O_3 dosage (Fig. 8a) can be related to higher rate of O_3 mass transfer in the membrane ozonation reactor [56]. The highly stable organic compound MLN and short-chain perfluoroalkylated substances-PFAS (PFBA, PFOA, PFBS, TFMS) showed a low reactivity with ozone even at higher ozone doses (OD$_I$ = 18 g m^{-3}; TOD = 7.1 g m^{-3}). Studies on the degradation of the MLN compound are still

lacking, especially with O_3. Maurino et al. [57] tested several advanced oxidation processes to remove MLN and concluded that only photocatalysis and the generation of $SO_4^{\bullet-}$ are capable of transforming MLN. They indicated that the primary photocatalytic event is the oxidation of the amino group, which reacts slowly with O_3 [58]. For the poor removal of PFAS, a possible explanation may be the low reactivity with O_3, indicating that large amounts of energy are required for their degradation [59]. The recalcitrance of PFAS towards ozonation is due to their strong carbon–fluorine bonds that make this compound a very stable and resistant pollutant. Other authors have also reported that ozonation has been shown to be relatively ineffective for PFAS destruction even with a long residence time [60–62]. As the membrane contactor was designed to evaluate the interaction of the photocatalytic ozonation process, the O_3/UVC/TiO$_2$ process was also performed to promote the generation of hydroxyl radical species (Fig. 8b). Nonetheless, the removal of MLN or PFAS was not improved. The low residence time (3.9 s) and UVC fluence (50 mJ cm^{-2}) applied in this treatment, resulting in a considerably lower UV dose than those normally used in WWTP [63], may be acting as limiting factor for the effective oxidation
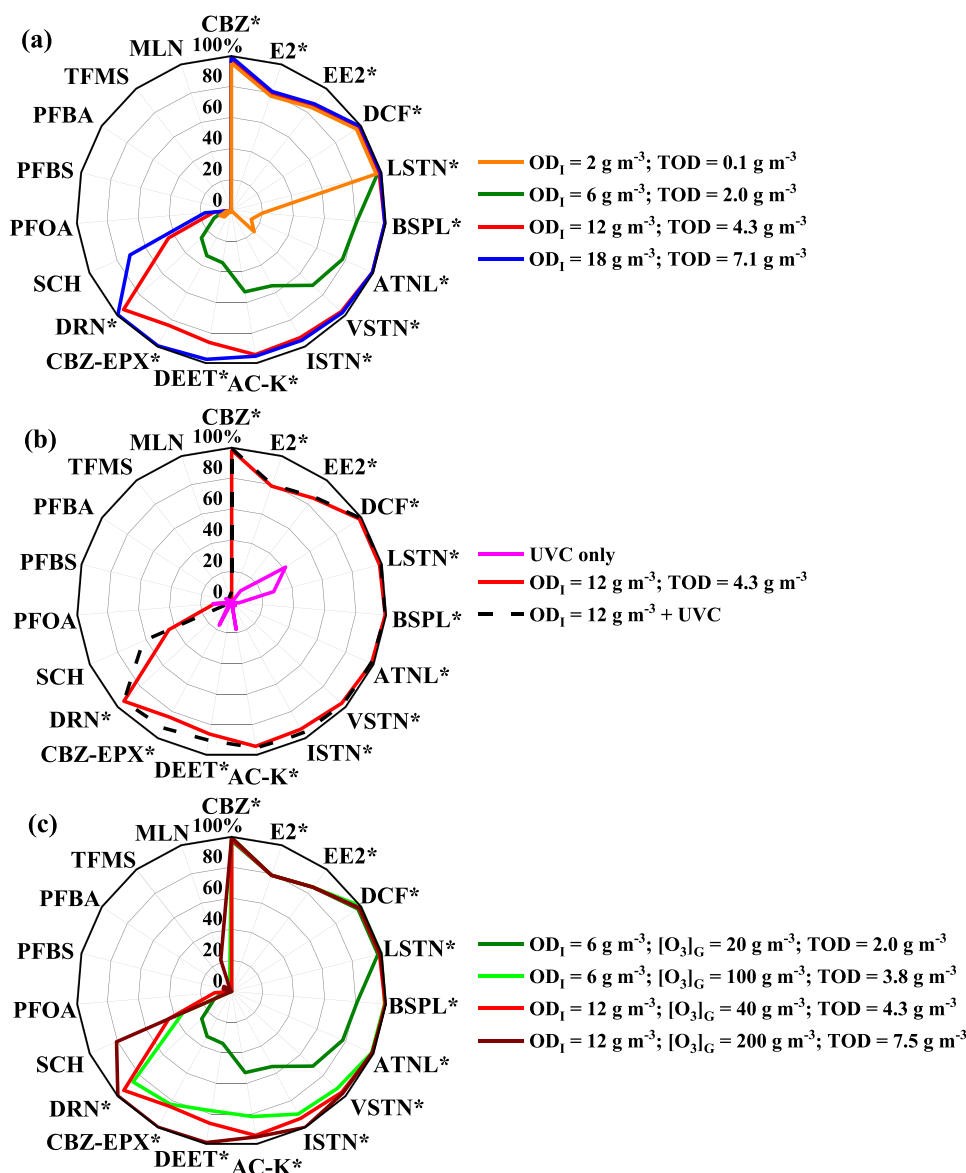

Fig. 8. CECs removal in continuous mode: effect of (a) ozone dosage, (b) UVC/TiO$_2$ process and (c) inlet ozone concentration in the gas stream. Conditions: DW spiked with CECs (10 μg L^{-1} of each CEC); T = 20 °C; pH = 6.5; Q_G = 0.15 and 0.75 Ndm^3 min^{-1}; Q_L = 150 L h^{-1}; [O$_3$]$_G$ = 20, 40, 100 and 200 g Nm^{-3}. * The removal values are presented as the maximum percentage that can be determined, taking into account the limits of quantification of the analytical method (Table S3).

of these compounds. This is underlined by the experiment without ozone (photocatalysis, UVC/TiO₂), where negligible removals (<10%) for all CECs were obtained. On the other hand, O₃/UVC/TiO₂ process had a slightly better removal efficiency than the ozonation for SCH (from 44% to 62%), which can be related to the greater amount of hydroxyl radicals available in the medium, since SCH shows high reactivity with this radical [64].

To further assess the ozonation treatment, tests were carried out for two O₃ doses (OD$_I$ of 6 or 12 g m^{-3}) and for each two O₃-gas flow rates (Q$_G$ of 0.15 or 0.75 L min^{-1}) (Fig. 8c). For the same OD$_I$ it is advantageous to reduce the Q$_G$ while increasing the ozone-gas concentration applied to the treatment. Since the main driving force for ozone mass transfer is the concentration difference in the gas–liquid two-phase. This indicates that more O₃ is being transferred from the gaseous to the liquid phase as a result of the increase in [O₃]$_G$ [65] and, consequently, the degradation rate of CECs is promoted (Fig. 8c).

Another important factor in the interpretation of results is the determination of the Hatta number (*Ha*), a recognized necessary standard that provides information about the competition between reaction kinetics and the rate of mass transfer [66]. As seen previously (*Section 3.2.2*), the mass transfer mechanism in the ozone membrane contactor can be divided into three regions (gaseous phase, membrane, and liquid phase). Therefore, *Ha* is the criterion for determining where the reaction occurs. In the present study, the data required to calculate this number can only be obtained for 13 of the 19 CECs, i.e., those that were effectively removed with ozonation (for OD_I = 12 g m^{-3}, Q_G = 0.75 Ndm^3 min^{-1}; Q_L = 150 L h^{-1}). These 13 CECs were divided into 8 groups due to their similarity. To identify the reaction regime and place during the reaction between CECs and dissolved ozone, the *Ha* is given by (Eq. 14) [67]:

$$Ha = \frac{\sqrt{k_{O3} \times Dw_{O3} \times [CECs]_0}}{k_L} \qquad (14)$$

where k_{O3} is the rate constant of the direct reaction between ozone and the pollutant (M^{-1} s^{-1}), Dw_{O3} is the diffusivity of ozone in water (1.76 × 10^{-9} m^2 s^{-1}) [68], [CECs]$_0$ is the CECs concentration in the feed liquid stream (M) and k_L is the ozone mass transfer coefficient to the liquid (K_L cannot be considered due to the high mass transfer resistance in the membrane – *Section 3.2.2*). Since the reaction is with a mixture of 13 CECs, the k_{O3} value adopted for each group was that of the chemical with the lowest rate constant, as it will limit the overall reaction rate (see Table S4). The k_L of 4.8 × 10^{-5} m s^{-1} was calculated considering the value of K_La obtained in our study for the experimental conditions used in the CECs ozonation. The *Ha* values obtained for the studied compounds were below 0.5 (Table S4). According to Charpentier [69], this corresponds to a moderate reaction, which occurs both in the liquid film and in the liquid bulk. The most recommended reactors to promote this type of reaction have high interfacial area and high liquid retention time. In the present study, the tubular porous borosilicate membrane contactor gave a high interfacial area (2131.6 m^{-1}) and a short liquid retention time (3.9 s), an advantageous feature when treating effluents with high flow rates, such as urban wastewater.

4. Conclusions

This study has proven the viability of using a tubular porous borosilicate membrane contactor for radial delivery of O₃, promoting intensification of ozone mass transfer in a compact device and this was applied for the removal of CECs in water. The pseudo-uniform feed distribution of O₃ along the length of an annular membrane creates innumerable micro-sized bubbles, increasing the surface area of the O₃ bubble in contact with the liquid allowing for a controlled "titration" of O₃ to the water-side.

Operating in continuous mode and under atmospheric pressure, the K_La values for this membrane reactor (3.5 – 9.0 min^{-1}) were comparable

to that of a venturi injector and were superior to other membrane contactors reported in the literature. The significant enhancements obtained for K_La and MTE using this ozone membrane contactor with low gas/liquid volumetric ratios, make this type of contactor highly effective for ozone gas/water mass transfer in water treatment.

This ozone membrane contactor was also proven to perform effectively for the treatment of water/wastewater by ozone-based processes and removals above 80% were achieved in 13 of the 19 selected CECs. In this case, the application of photocatalytic ozonation (O₃/UVC/TiO₂) did not significantly improve the removal of CECs. Not with standing, the versatility of this setup, allowing the membrane to be doped with a catalyst and operated under UVC radiation, may prove advantageous when treating highly complex wastewater matrices.

CRediT authorship contribution statement

Pedro H. Presumido: Conceptualization, Methodology, Investigation; Writing – original draft preparation. **Rosa Montes:** Methodology; Writing – review & editing. **José B. Quintana:** Resources; Writing – review & editing. **Rosario Rodil:** Resources; Writing – review & editing. **Manuel Feliciano:** Supervision, Writing – review & editing. **Gianluca Li Puma:** Writing – review & editing. **Ana I. Gomes:** Conceptualization, Methodology, Supervision, Writing – review & editing. **Vítor J. P. Vilar:** Conceptualization, Methodology, Resources, Supervision, Writing – review & editing.

Declaration of Competing Interest

The authors declare that they have no known competing financial interests or personal relationships that could have appeared to influence the work reported in this paper.

Acknowledgements

Appendix A. Supporting information

Supplementary data associated with this article can be found in the online version at doi:10.1016/j.jece.2022.108671.

References

[1] C. Gottschalk, J.A. Libra, A. Saupe, Ozonation of water and waste water: A practical guide to understanding ozone and its applications, 2nd Edition, Wiley-VCH Verlag GmbH & Co. kGaA, Germany, 2010.

[2] S. Ribeirinho-Soares, N.F.F. Moreira, C. Graça, M.F.R. Pereira, A.M.T. Silva, O. C. Nunes, Overgrowth control of potentially hazardous bacteria during storage of ozone treated wastewater through natural competition, Water Res. 209 (2022), 117932, https://doi.org/10.1016/j.watres.2021.117932.

[3] T. Spit, J.P. van der Hoek, C. de Jong, D. van Halem, M. de Kreuk, B.B. Perez, Removal of antibiotic resistance from municipal secondary effluents by ozone-activated carbon filtration, Front. Environ. Sci. 10 (2022), https://doi.org/10.3389/fenvs.2022.834577.

[4] T. Merle, W. Pronk, U. von Gunten, MEMBRO3X, a novel combination of a membrane contactor with advanced oxidation (O_3/H_2O_2) for simultaneous micropollutant abatement and bromate minimization, Environ. Sci. Technol. Lett. 4 (5) (2017) 180–185, https://doi.org/10.1021/acs.estlett.7b00061.

[5] F. Smuts, C. Gaszynski, D. Ikumi, A framework to determine the optimum contact time and organic micropollutant removal efficiency of the ozone process applied in the context of cape flats managed aquifer recharge water reclamation plant, J. Water Process Eng. 47 (2022), 102651, https://doi.org/10.1016/j.jwpe.2022.102651.

[6] B. Mathon, M. Coquery, Z. Liu, Y. Penru, A. Guillon, M. Esperanza, C. Miège, J. M. Choubert, Ozonation of 47 organic micropollutants in secondary treated municipal effluents: direct and indirect kinetic reaction rates and modelling, Chemosphere 262 (2021), 127969, https://doi.org/10.1016/j.chemosphere.2020.127969.

[7] Z.A. Yacouba, J. Mendret, G. Lesage, F. Zaviska, S. Brosillon, Removal of organic micropollutants from domestic wastewater: the effect of ozone-based advanced oxidation process on nanofiltration, J. Water Process Eng. 39 (2021), 101869, https://doi.org/10.1016/j.jwpe.2020.101869.

[8] C. Anselme, I.H. Suffet, J. Mallevialle, Effects of ozonation on tastes and odors, J. Am. Water Works Assoc. 80 (10) (1988) 45–51.

[9] B.L. Loeb, Forty years of advances in ozone technology. a review of ozone: science & engineering, Ozone Sci. Eng. 40 (1) (2018) 3–20, https://doi.org/10.1080/01919512.2017.1383129.

[10] K.K. Sirkar, Membranes, phase interfaces, and separations: novel techniques and membranes—an overview, Ind. Eng. Chem. Res. 47 (15) (2008) 5250–5266, https://doi.org/10.1021/ie8001952.

[11] E. Bein, I. Zucker, J.E. Drewes, U. Hübner, Ozone membrane contactors for water and wastewater treatment: a critical review on materials selection, mass transfer and process design, Chem. Eng. J. 413 (2021), 127393, https://doi.org/10.1016/j.cej.2020.127393.

[12] A.K. Pabby, A.M. Sastre, State-of-the-art review on hollow fibre contactor technology and membrane-based extraction processes, J. Membr. Sci. 430 (2013) 263–303, https://doi.org/10.1016/j.memsci.2012.11.060.

[13] A. Mansourizadeh, A.F. Ismail, Hollow fiber gas–liquid membrane contactors for acid gas capture: a review, J. Hazard. Mater. 171 (1) (2009) 38–53, https://doi.org/10.1016/j.jhazmat.2009.06.026.

[14] K. Li, L. Xu, Y. Zhang, A. Cao, Y. Wang, H. Huang, J. Wang, A novel electro-catalytic membrane contactor for improving the efficiency of ozone on wastewater treatment, Appl. Catal. B Environ. 249 (2019) 316–321, https://doi.org/10.1016/j.apcatb.2019.03.015.

[15] A. Schmitt, J. Mendret, M. Roustan, S. Brosillon, Ozonation using hollow fiber contactor technology and its perspectives for micropollutants removal in water: a review, Sci. Total Environ. 729 (2020), 138664, https://doi.org/10.1016/j.scitotenv.2020.138664.

[16] W.J. Lee, Y. Bao, A. Liangdy, X. Hu, T.-T. Lim, Insights into the synergistic role of catalytic ceramic membranes for ozone and peroxymonosulfate activation towards effective recalcitrant micropollutant degradation and mineralization, Chem. Eng. J. 430 (2022), 132921, https://doi.org/10.1016/j.cej.2021.132921.

[17] Y. Liu, Z. Song, W. Wang, Z. Wang, Y. Zhang, C. Liu, Y. Wang, A. Li, B. Xu, F. Qi, A CuMn$_2$O$_4$/g-C$_3$N$_4$ catalytic ozonation membrane reactor used for water purification: Membrane fabrication and performance evaluation, Sep. Purif. Technol. 265 (2021), 118268, https://doi.org/10.1016/j.seppur.2020.118268.

[18] C. Mansas, L. Atfane-Karfane, E. Petit, J. Mendret, S. Brosillon, A. Ayral, Functionalized ceramic nanofilter for wastewater treatment by coupling membrane separation and catalytic ozonation, J. Environ. Chem. Eng. 8 (4) (2020), 104043, https://doi.org/10.1016/j.jece.2020.104043.

[19] Y. Li, K.L. Yeung, Polymeric catalytic membrane for ozone treatment of DEET in water, Catal. Today 331 (2019) 53–59, https://doi.org/10.1016/j.cattod.2018.06.005.

[20] F.C. Moreira, E. Bocos, A.G.F. Faria, J.B.L. Pereira, C.P. Fonte, R.J. Santos, J.C. B. Lopes, M.M. Dias, M.A. Sanromán, M. Pazos, R.A.R. Boaventura, V.J.P. Vilar, Selecting the best piping arrangement for scaling-up an annular channel reactor: an experimental and computational fluid dynamics study, Sci. Total Environ. 667 (2019) 821–832, https://doi.org/10.1016/j.scitotenv.2019.02.260.

[21] American Public Health Association, Standard methods for the examination of water and wastewater, 19th ed., American Public Health Association, Washington, D.C, 1995.

[22] C.M. Birdsall, A.C. Jenkins, E. Spadinger, Iodometric determination of ozone, Anal. Chem. 24 (4) (1952) 662–664, https://doi.org/10.1021/ac60064a013.

[23] J.Fd.S. Petruci, D.N. Barreto, M.A. Dias, E.P. Felix, A.A. Cardoso, Analytical methods applied for ozone gas detection: a review, TrAC Trends Anal. Chem. 149 (2022), 116552, https://doi.org/10.1016/j.trac.2022.116552.

[24] M. Griggs, Absorption coefficients of ozone in the ultraviolet and visible regions, J. Chem. Phys. 49 (2) (1968) 857–859, https://doi.org/10.1063/1.1670152.

[25] C.G. Hatchard, C.A. Parker, E.J. Bowen, A new sensitive chemical actinometer - II. Potassium ferrioxalate as a standard chemical actinometer, Proc. R. Soc. Lond. Ser. A. Math. Phys. Sci. 235 (1203) (1956) 518–536, https://doi.org/10.1098/rspa.1956.0102.

[26] J. Rabani, H. Mamane, D. Pousty, J.R. Bolton, Practical chemical actinometry—a review, Photochem. Photobiol. 97 (5) (2021) 873–902, https://doi.org/10.1111/php.13429.

[27] P.H. Presumido, L.Fd Santos, T. Neuparth, M.M. Santos, M. Feliciano, A. Primo, H. Garcia, M. B- Đolić, V.J.P. Vilar, A Novel ceramic tubular membrane coated with a continuous graphene-TiO2 nanocomposite thin-film for CECs mitigation, Chem. Eng. J. 430 (2022), 132639, https://doi.org/10.1016/j.cej.2021.132639.

[28] T. Liu, D. Wang, W. Wang, Q. Liang, L. Shao, Study on the efficient production of ozone water by a rotating packed bed, Ind. Eng. Chem. Res. 58 (17) (2019) 7227–7232, https://doi.org/10.1021/acs.iecr.8b06486.

[29] M. Kukuzaki, K. Fujimoto, S. Kai, K. Ohe, T. Oshima, Y. Baba, Ozone mass transfer in an ozone–water contacting process with Shirasu porous glass (SPG) membranes—A comparative study of hydrophilic and hydrophobic membranes, Sep. Purif. Technol. 72 (3) (2010) 347–356, https://doi.org/10.1016/j.seppur.2010.03.004.

[30] A. Gabelman, S.-T. Hwang, Hollow fiber membrane contactors, J. Membr. Sci. 159 (1) (1999) 61–106, https://doi.org/10.1016/S0376-7388(99)00040-X.

[31] P.N. Johnson, R.A. Davis, Diffusivity of ozone in water, J. Chem. Eng. Data 41 (6) (1996) 1485–1487, https://doi.org/10.1021/je9602125.

[32] S. Bamperng, T. Suwannachart, S. Atchariyawut, R. Jiraratananon, Ozonation of dye wastewater by membrane contactor using PVDF and PTFE membranes, Sep. Purif. Technol. 72 (2) (2010) 186–193, https://doi.org/10.1016/j.seppur.2010.02.006.

[33] M. Sommerfeld, D. Bröder, Analysis of hydrodynamics and microstructure in a bubble column by planar shadow image velocimetry, Ind. Eng. Chem. Res. 48 (1) (2009) 330–340, https://doi.org/10.1021/ie800838u.

[34] J.A. Roth, D.E. Sullivan, Solubility of ozone in water, Ind. Eng. Chem. Fundam. 20 (2) (1981) 137–140, https://doi.org/10.1021/i100002a004.

[35] H. Tomiyasu, H. Fukutomi, G. Gordon, Kinetics and mechanism of ozone decomposition in basic aqueous solution, Inorg. Chem. 24 (19) (1985) 2962–2966, https://doi.org/10.1021/ic00213a018.

[36] Y. Jung, E. Hong, M. Kwon, J.-W. Kang, A kinetic study of ozone decay and bromine formation in saltwater ozonation: Effect of O_3 dose, salinity, pH, and temperature, Chem. Eng. J. 312 (2017) 30–38, https://doi.org/10.1016/j.cej.2016.11.113.

[37] U. von Gunten, Ozonation of drinking water: part I. Oxidation kinetics and product formation, Water Res. 37 (7) (2003) 1443–1467, https://doi.org/10.1016/S0043-1354(02)00457-8.

[38] R. Rosal, A. Rodríguez, M. Zerhouni, Enhancement of gas–liquid mass transfer during the unsteady-state catalytic decomposition of ozone in water, Appl. Catal. A: Gen. 305 (2) (2006) 169–175, https://doi.org/10.1016/j.apcata.2006.02.059.

[39] B. Wang, X. Xiong, Y. Shui, Z. Huang, K. Tian, A systematic study of enhanced ozone mass transfer for ultrasonic-assisted PTFE hollow fiber membrane aeration process, Chem. Eng. J. 357 (2019) 678–688, https://doi.org/10.1016/j.cej.2018.09.188.

[40] R.C. Martins, R.J.G. Lopes, R.M. Quinta-Ferreira, Lumped kinetic models for single ozonation of phenolic effluents, Chem. Eng. J. 165 (2) (2010) 678–685, https://doi.org/10.1016/j.cej.2010.09.060.

[41] J.C.G. Peres, Ud Silvio, A.C.S.C. Teixeira, R. Guardani, Ad.S.V. Jr, Study of an annular photoreactor with tangential inlet and outlet: I. Fluid dynamics, Chem. Eng. Technol. 38 (2) (2015) 311–318, https://doi.org/10.1002/ceat.201400186.

[42] G.T. Vladisavljević, Use of polysulfone hollow fibers for bubbleless membrane oxygenation/deoxygenation of water, Sep. Purif. Technol. 17 (1) (1999) 1–10, https://doi.org/10.1016/S1383-5866(99)00012-X.

[43] K. Li, Y. Zhang, L. Xu, L. Liu, Z. Wang, D. Hou, Y. Wang, J. Wang, Mass transfer and interfacial reaction mechanisms in a novel electro-catalytic membrane contactor for wastewater treatment by O_3, Appl. Catal. B Environ. 264 (2020), 118512, https://doi.org/10.1016/j.apcatb.2019.118512.

[44] S.B. Iversen, V.K. Bhatia, K. Dam-Johansen, G. Jonsson, Characterization of microporous membranes for use in membrane contactors, J. Membr. Sci. 130 (1) (1997) 205–217, https://doi.org/10.1016/S0376-7388(97)00026-4.

[45] R.H.S. Jansen, J.W. de Rijk, A. Zwijnenburg, M.H.V. Mulder, M. Wessling, Hollow fiber membrane contactors—A means to study the reaction kinetics of humic substance ozonation, J. Membr. Sci. 257 (1) (2005) 48–59, https://doi.org/10.1016/j.memsci.2004.07.038.

[46] M. Mavroudi, S.P. Kaldis, G.P. Sakellaropoulos, A study of mass transfer resistance in membrane gas–liquid contacting processes, J. Membr. Sci. 272 (1) (2006) 103–115, https://doi.org/10.1016/j.memsci.2005.07.025.

[47] A. Al-Abduly, P. Christensen, A. Harvey, K. Zahng, Characterization and optimization of an oscillatory baffled reactor (OBR) for ozone-water mass transfer, Chem. Eng. Process. Process.Intensif. 84 (2014) 82–89, https://doi.org/10.1016/j.cep.2014.03.015.

[48] X. Huang, X. Quan, W. Cheng, C. Cheng, Z. Cheng, L. Yang, L. Jiang, Enhancement of ozone mass transfer by stainless steel wire mesh and its effect on hydroxyl radical generation, Ozone.: Sci. Eng. 42 (4) (2020) 347–356, https://doi.org/10.1080/01919512.2019.1676196.

[49] A.K. Bín, B. Duczmal, P. Machniewski, Hydrodynamics and ozone mass transfer in a tall bubble column, Chem. Eng. Sci. 56 (21) (2001) 6233–6240, https://doi.org/10.1016/S0009-2509(01)00213-5.

[50] M.S. Baawain, M. Gamal El-Din, D.W. Smith, A. Mazzei, Hydrodynamic characterization and mass transfer analysis of an in-line multi-jets ozone contactor, Ozone.: Sci. Eng. 33 (6) (2011) 449–462, https://doi.org/10.1080/01919512.2011.622705.

[51] C. Tizaoui, Y. Zhang, The modelling of ozone mass transfer in static mixers using Back Flow Cell Model, Chem. Eng. J. 162 (2) (2010) 557–564, https://doi.org/10.1016/j.cej.2010.05.061.

[52] D.S. Pines, K.-N. Min, S.J. Ergas, D.A. Reckhow, Investigation of an ozone membrane contactor system, Ozone Sci. Eng. 27 (3) (2005) 209–217, https://doi.org/10.1080/01919510590945750.

[53] M.S. Lucas, N.M. Reis, G. Li Puma, Intensification of ozonation processes in a novel, compact, multi-orifice oscillatory baffled column, Chem. Eng. J. 296 (2016) 335–339, https://doi.org/10.1016/j.cej.2016.03.050.

[54] X. Liu, X. Su, S. Tian, Y. Li, R. Yuan, Mechanisms for simultaneous ozonation of sulfamethoxazole and natural organic matters in secondary effluent from sewage treatment plant, Front. Environ. Sci. Eng. 15 (4) (2020) 75, https://doi.org/10.1007/s11783-020-1368-0.

[55] J. Wang, H. Chen, Catalytic ozonation for water and wastewater treatment: recent advances and perspective, Sci. Total Environ. 704 (2020), 135249, https://doi.org/10.1016/j.scitotenv.2019.135249.

[56] K. Yaghmaeian, G. Moussavi, A. Mashayekh-Salehi, A. Mohseni-Bandpei, M. Satari, Oxidation of acetaminophen in the ozonation process catalyzed with modified MgO nanoparticles: effect of operational variables and cytotoxicity assessment, Process Saf. Environ. Prot. 109 (2017) 520–528, https://doi.org/10.1016/j.psep.2017.04.020.

[57] V. Maurino, M. Minella, F. Sordello, C. Minero, A proof of the direct hole transfer in photocatalysis: the case of melamine, Appl. Catal. A Gen. 521 (2016) 57–67, https://doi.org/10.1016/j.apcata.2015.11.012.

[58] W.A. Pryor, D.H. Giamalva, D.F. Church, Kinetics of ozonation. 2. Amino acids and model compounds in water and comparisons to rates in nonpolar solvents, J. Am. Chem. Soc. 106 (23) (1984) 7094–7100, https://doi.org/10.1021/ja00335a038.

[59] M. Alameddine, A. Siraki, L. Tonoyan, M. Gamal El-Din, Treatment of a mixture of pharmaceuticals, herbicides and perfluorinated compounds by powdered activated carbon and ozone: synergy, catalysis and insights into non-free OH contingent mechanisms, Sci. Total Environ. 777 (2021), 146138, https://doi.org/10.1016/j.scitotenv.2021.146138.

[60] V. Franke, M.D. Schäfers, J. Joos Lindberg, L. Ahrens, Removal of per- and polyfluoroalkyl substances (PFASs) from tap water using heterogeneously catalyzed ozonation, Environ. Sci. Water Res. Technol. 5 (11) (2019) 1887–1896, https://doi.org/10.1039/C9EW00339H.

[61] H.F. Schröder, R.J.W. Meesters, Stability of fluorinated surfactants in advanced oxidation processes—A follow up of degradation products using flow injection–mass spectrometry, liquid chromatography–mass spectrometry and liquid chromatography–multiple stage mass spectrometry, J. Chromatogr. A 1082 (1) (2005) 110–119, https://doi.org/10.1016/j.chroma.2005.02.070.

[62] C.D. Vecitis, H. Park, J. Cheng, B.T. Mader, M.R. Hoffmann, Treatment technologies for aqueous perfluorooctanesulfonate (PFOS) and perfluorooctanoate (PFOA), Front. Environ. Sci. Eng. China 3 (2) (2009) 129–151, https://doi.org/10.1007/s11783-009-0022-7.

[63] C.P. James, E. Germain, S. Judd, Micropollutant removal by advanced oxidation of microfiltered secondary effluent for water reuse, Sep. Purif. Technol. 127 (2014) 77–83, https://doi.org/10.1016/j.seppur.2014.02.016.

[64] C. Ye, X. Ma, J. Deng, X. Li, Q. Li, A.M. Dietrich, Degradation of saccharin by UV/H₂O₂ and UV/PS processes: a comparative study, Chemosphere 288 (2022), 132337, https://doi.org/10.1016/j.chemosphere.2021.132337.

[65] J. Ren, S. He, C. Ye, G. Chen, C. Sun, The ozone mass transfer characteristics and ozonation of pentachlorophenol in a novel microchannel reactor, Chem. Eng. J. 210 (2012) 374–384, https://doi.org/10.1016/j.cej.2012.09.011.

[66] M.S. Lucas, J.A. Peres, B.Y. Lan, G. Li Puma, Ozonation kinetics of winery wastewater in a pilot-scale bubble column reactor, Water Res. 43 (6) (2009) 1523–1532, https://doi.org/10.1016/j.watres.2008.12.036.

[67] H. Benbelkacem, H. Cano, S. Mathe, H. Debellefontaine, Maleic acid ozonation: reactor modeling and rate constants determination, Ozone.: Sci. Eng. 25 (1) (2003) 13–24, https://doi.org/10.1080/713610647.

[68] P.N. Johnson, R.A. Davis, Diffusivity of ozone in water, J. Chem. Eng. Data 41 (6) (1997) 1485–1487, https://doi.org/10.1021/je9602125.

[69] J.-C. Charpentier, Mass-Transfer Rates in Gas-Liquid Absorbers and Reactors, in: T. B. Drew, G.R. Cokelet, J.W. Hoopes, T. Vermeulen (Eds.), Advances in Chemical Engineering, Academic Press, 1981, pp. 1–133. https://doi.org/10.1016/S0065-2377(08)60025-3.

[70] G.A. Zoumpouli, R. Baker, C.M. Taylor, M.J. Chippendale, C. Smithers, S.S.X. Ho, D. Mattia, Y.M.J. Chew, J. Wenk, A single tube contactor for testing membrane ozonation, Water 10 (10) (2018) 1416, https://doi.org/10.3390/w10101416.

[71] B. Wang, H. Zhang, Q. Meng, H. Ren, M. Xiong, C. Gao, The enhancement of ozone–liquid mass transfer performance in a PTFE hollow fiber membrane contactor using ultrasound as a catalyzer, RSC Adv. 11 (23) (2021) 14017–14028, https://doi.org/10.1039/D1RA00452B.